energies

MDPI

Article

Forecasting China's Crude Oil Futures Price by Recurrent Neural Network Method Based on Unconstrained Transformation

Yixuan Zhu [1], Wenhao Yao [2] and Tianhui Fang [3,*]

[1] School of Statistics and Data Science, Shanghai University of Finance and Economic, Shanghai 200433, China; 2019111507@stu.sufe.edu.cn
[2] Wanhua Chemical Group Co., Ltd., Yantai 264002, China; yaowh0202@163.com
[3] School of Business, Shanghai University of Finance and Economic, Shanghai 200433, China
* Correspondence: 15921011580@163.com; Tel.: +86-159-2101-1580

Abstract

This study examines whether a structure-preserving representation of the joint Open-High-Low-Close (OHLC) vector provides coherent forecasts for China's INE crude-oil futures and how seven benchmark models compare within that representation. The sample contains 1547 trading days from the contract launch to 8 January 2025. Under the originally reported 80:20 setting, GRU has the smallest aggregate MAPE (0.7825%), MAE (4.6774), and RMSE (7.2957), together with the largest interval-overlap Success Ratio (0.5629). These figures establish a numerical ranking only: the archived materials do not verify the exact temporal split, training-only preprocessing, component-specific errors, or price-limit-event robustness. The economic section therefore contains only illustrative Close-to-Close and Open-to-Close mappings and does not claim executable profitability. The defensible contribution is the structure-preserving OHLC framework and a bounded numerical comparison.

Keywords: OHLC data; INE crude oil; unconstrained transformation method; gated recurrent unit network

1. Introduction

Crude oil is a major input to industrial production, transport, and household energy use [1–5]. China is both the largest crude-oil importer and one of the world's largest oil consumers [6,7]; so, oil-price movements can affect input costs, inflation expectations, hedging decisions, and financial-market risk [8]. The financialization of the commodity also links futures prices with information from currency, equity, commodity, and interest-rate markets [9].

China's Shanghai International Energy Exchange crude-oil contract began trading on 26 March 2018 and has become an important Asian benchmark setting [10–13]. Its expanding activity and renminbi denomination connect the contract with regional price discovery and risk transmission, although its international pricing influence is still developing. The market therefore provides a useful setting for a forecasting design that accounts for both domestic and global financial conditions [10–13].

Forecasting this contract is complicated by non-stationarity, nonlinear dynamics, volatility clustering, structural change, and abrupt external shocks [14–21]. The pandemic [22], changes in OPEC policy, and the Russia–Ukraine conflict illustrate why relationships estimated in one market regime may not persist in another. An informative evaluation must consequently preserve chronology, keep future information out of model construction, and report performance across distinct market conditions.

Check for updates

Academic Editor: Dameng Liu

Received: 25 July 2026
Revised: 6 September 2026
Accepted: 15 September 2026
Published: 18 September 2026

Copyright: © 2026 by the authors. Licensee MDPI, Basel, Switzerland. This article is an open access article distributed under the terms and conditions of the Creative Commons Attribution (CC BY) license.

The contract also operates under exchange-specific restrictions. Daily price limits can prevent execution when a contract is locked and counterparties are unavailable. Independently, an OHLC vector must satisfy the ordering conditions that the low cannot exceed the open or close and the high cannot be below them. The forecasting representation should preserve these structural relations, while the interpretation of any trading calculation must remain separate from legal price-limit and liquidity feasibility [23,24].

Much of the crude-oil forecasting literature models a single closing-price series or transforms that series to improve point forecasts [25–27]. Such designs omit the opening price and the intraday range. Interval-valued approaches retain some high-low information, but they do not always represent all four OHLC components or evaluate their separate economic roles [23,28–32]. In addition, reported forecast accuracy is sometimes linked directly to profitability without a full account of information timing, execution order, transaction frictions, or downside exposure [33].

This study has three objectives. First, it applies an unconstrained transformation that retains the internal relations of the INE OHLC vector. Second, it compares linear, machine-learning, and recurrent-neural benchmarks under the reported evaluation setting. Third, it uses the predicted OHLC components to illustrate economic decision rules while distinguishing potentially observable rules from ex-post scenarios that require knowledge of daily extrema. The external financial series are descriptive context rather than inputs to the reported forecasting models. Accordingly, the study does not claim that its forecasts stabilize the economy, improve liquidity, remove crisis risk, or constitute investor-ready trading performance.

2. Literature Review

Crude-oil futures are highly volatile, and this volatility has motivated a broad forecasting literature [34]. Before China's contract was listed in 2018, much of the evidence concerned WTI and Brent; subsequent work has increasingly examined INE prices and volatility [1,35–37]. Existing studies can be grouped into linear econometric methods, machine-learning methods, and hybrid designs, while another stream investigates the market variables associated with oil-price movements [15,38].

Traditional work uses linear regression, GARCH, ARIMA, VAR, and VECM to describe price dynamics [39,40]. These models offer interpretable economic relationships but rely on stronger assumptions and may have difficulty representing highly volatile nonlinear series [2]. Recent examples extend ARIMA with Baidu search attention and report predictive information in the feed index [41], document an intraday reversal effect in high-frequency INE returns [42], and use VECM and DAG to study the pricing power and hedging role of the INE contract in Asian price transmission [43].

The availability of high-frequency observations and artificial-intelligence methods has broadened energy-finance forecasting research [44,45]. Neural and other nonlinear learners can represent relationships that are difficult to capture with linear specifications. In a comparison of seven artificial-intelligence models for daily INE data from 26 March 2018 to 28 February 2023, Guo et al. reported the strongest forecasting performance for GRU [2].

Other studies add information beyond prices. Jiang et al. combine sentiment signals from Baidu, Alibaba, and Tencent with machine-learning models and report the best result for an LSTM using a composite sentiment index [46]. He et al. introduce a pretrained Transformer-based language model and find improved INE forecasting accuracy [47]. Luo et al. combine deterministic forecasting, uncertainty analysis, multi-objective optimization, fuzzy theory, and econometric/artificial intelligence components; their study reports

an improvement of more than 50% over a benchmark in four major crude-oil futures markets [48].

The related literature treats the daily high-low interval as the forecasting object. For example, BEMD, interval MLP, and interval exponential-smoothing components have been combined to model interval prices and their trend and volatility information [28,29]. Further interval-forecasting studies emphasize the value of retaining uncertainty and instability in the observed process [30–32]. These approaches nevertheless do not provide a complete, structured model of all OHLC components, which limits their direct use for multiple intraday decision rules.

3. Data and Methodology

3.1. INE OHLC Data and External-Market Context

This study used daily OHLC prices for the INE crude-oil futures series from the contract's launch to 8 January 2025. After excluding dates with missing observations, the sample contained 1547 trading days. Figure 1 illustrates the candlestick representation, and Figure 2 shows the price history. For descriptive purposes, the sample contained relatively turbulent periods as well as more stable periods; these visual regimes were not used as substitutes for a formal, ex-ante volatility classification.

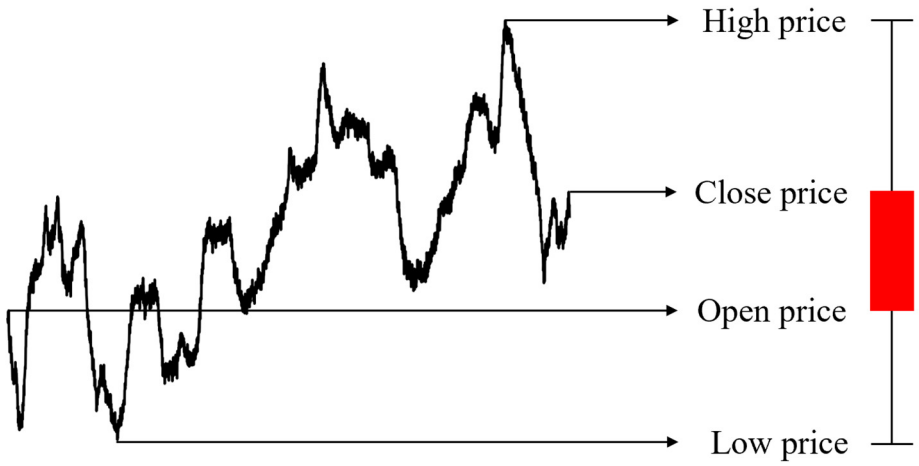

Figure 1. Candlestick chart. Note: the red rectangle represents the daily stock's real body gain.

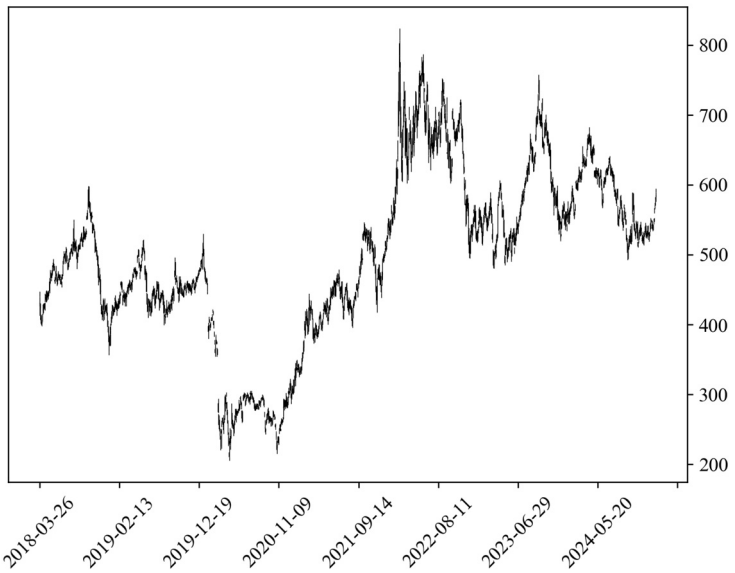

Figure 2. INE crude oil price chart.

From the Figure 3, we can find that the overall INE crude oil price is more volatile and susceptible to external extreme emergencies, for instance, COVID-19 at the beginning of 2020 and the Russia–Ukraine war, and the price has fluctuated rapidly, as shown in Figure 4. Subsequently, a series of emergencies in the international community still occurred frequently, but the overall political and economic situation in China remained stable, production resumed in an orderly manner, and the INE crude oil futures prices entered a phase of stable volatility, with the overall descriptive statistical indicators as shown in Table 1.

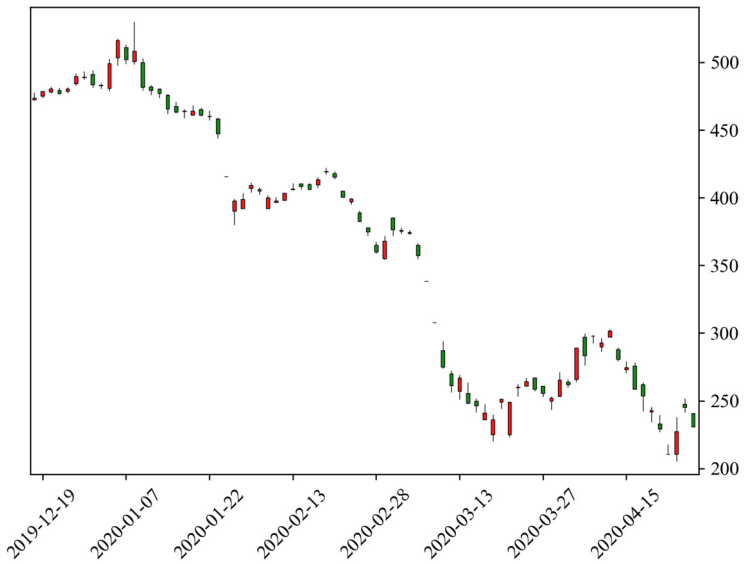

Figure 3. INE crude oil price crash chart. Note: Red indicates an increase, while green indicates a decrease.

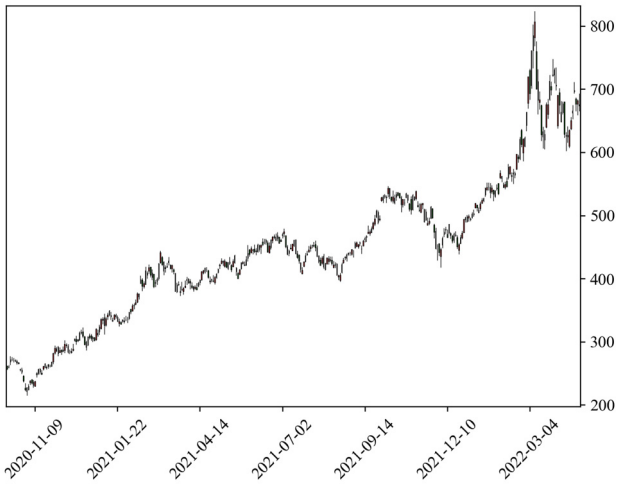

Figure 4. INE crude oil price spike chart.

Table 1. Statistical description of INE crude oil prices.

Price Type	Mean	Deviation	Minimum	Median	Maximum	Skewness	Kurtosis
Open price	496.87	122.12	210.60	501.30	781.90	−0.19	−0.44
Lowest price	490.04	120.47	205.30	495.30	768.20	−0.22	−0.45
Highest price	502.59	123.82	217.70	508.2	823.60	−0.16	−0.43
Close price	496.95	122.26	210.60	502.2	806.60	−0.19	−0.44

There are various influencing factors affecting changes in INE crude-oil futures prices, and this section describes selected variables from China's money, stock, and futures markets as market context [49]. These variables do not enter the seven forecasting models reported below.

Table 2 lists candidate predictors from the money, equity, and futures markets, while Figure 5 reports contemporaneous Pearson correlations for descriptive purposes. WTI crude-oil futures and SHFE bitumen exhibit the largest reported correlations with INE prices. These correlations do not establish incremental predictive content and are not a feature-selection result, because contemporaneous association may reflect common trends, non-stationarity, or information that was unavailable when the INE forecast was generated. The reported forecasting specifications use lagged transformed INE OHLC data only; no multivariate comparison is claimed.

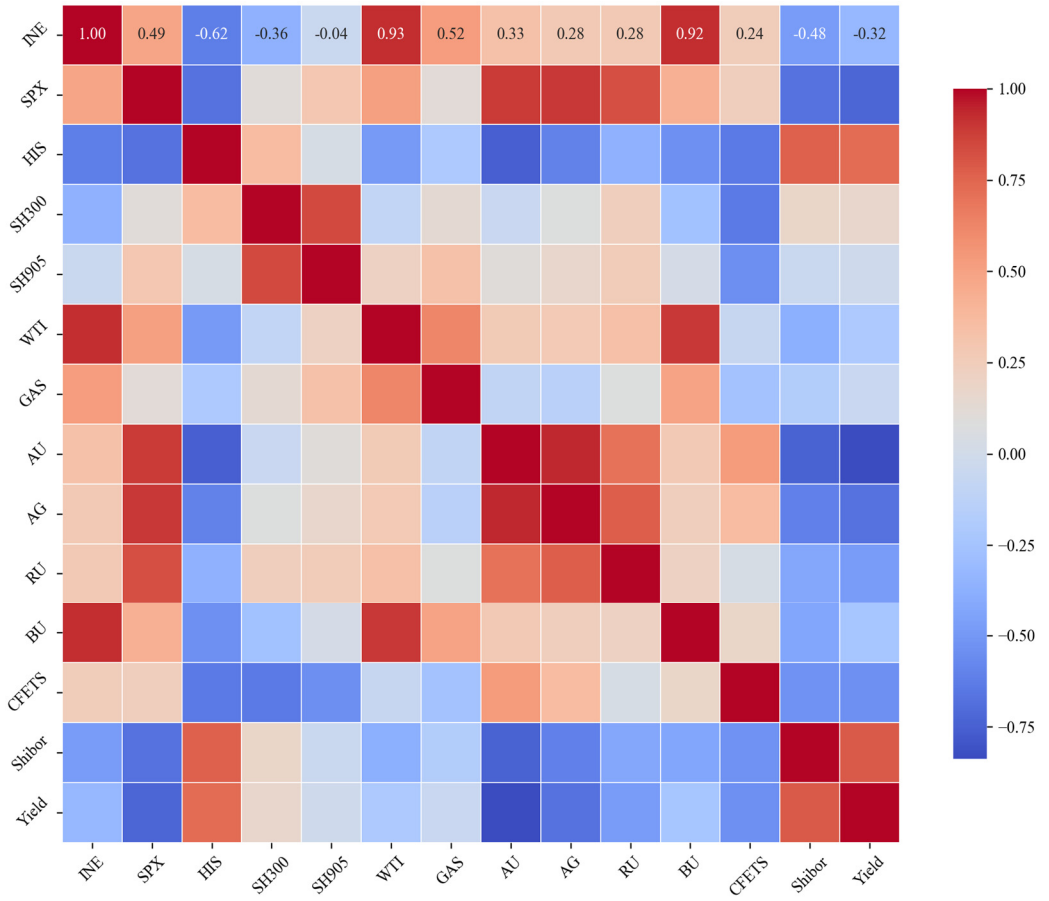

Figure 5. Heat map of correlation of influencing factors.

Predictor Availability and Information Set

For any future multivariate extension, predictor values must be restricted to information observable at the forecast cutoff. Domestic series should be aligned to their official release or market-close times. International prices whose trading sessions close after the INE decision time must enter with an additional lag; holidays and non-synchronous market closures must not be backfilled using future observations. Standardization, missing-value treatment, and any predictor selection must be fitted on the training period only and then applied without refitting to validation and test observations. These requirements are not part of the current OHLC-only specifications.

Table 2. Introduction to relevant influencing factors.

Types of Markets	Variable	Code	Data Type
Money market	China–US currency exchange rate	CFETS	OHLC
	Shibor 3-month lending rate	Shibor	Scale
	China's 3-year treasury bond interest rate	Yield	Scale
Stock market	S&P 500	SPX	OHLC
	Hang Seng Index	HIS	OHLC
	CSI 300	SH300	OHLC
	CSI 500	SH905	OHLC
Futures market	WTI crude oil futures	WTI	OHLC
	NEMEX natural gas futures	GAS	OHLC
	SHFE gold futures	AU	OHLC
	SHFE silver futures	AG	OHLC
	SHFE rubber futures	RU	OHLC
	SHFE bitumen futures	BU	OHLC

3.2. Methodological Framework

3.2.1. Unconstrained Transformation of OHLC Data

In this paper, a flexible and unrestrictedly applicable transformation method for OHLC data was used to represent it in the form of a vector that belongs to a 4 dimensional vector $X_t = \left(x_t^{(o)}, x_t^{(h)}, x_t^{(l)}, x_t^{(c)}\right)^T$, where the components represent the open, highest, lowest, and close prices during the day at moment t. The constraints that should also be satisfied are as follows:

1. Throughout the INE sample used in this study, the daily low is positive. We therefore applied a logarithmic transformation to the low-price component. This is a sample-specific property rather than a universal feature of crude-oil futures: WTI futures traded below zero in April 2020 under a different contract and market setting. Observations must not be deleted merely because they are economically inconvenient; any exclusion should follow a prespecified data-quality rule and be reported transparently. The first transformed component is defined in Equation (1).

$$y_t^{(1)} = \ln x_t^{(l)} \tag{1}$$

2. $x_t^{(l)} < x_t^{(h)}$, $x_t^{(o)}, x_t^{(c)} \in \left[x_t^{(l)}, x_t^{(h)}\right]$. Generally for the price of the day, the lowest price is lower than the highest prices, but also the day prices in the upper and lower boundaries, the open prices, and close prices are within the range of the prices' prediction results to meet the assumptions of this condition, the extreme case of $x_t^{(l)} = x_t^{(h)}$ considered in 3. Differencing the high and low prices and performing a logarithmic change yields $y_t^{(2)}$. Proxies $\lambda_t^{(o)}$ and $\lambda_t^{(c)}$ for the open and close prices, inspired by the convex portfolio, are obtained as follows:

$$y_t^{(2)} = \ln\left(x_t^{(h)} - x_t^{(l)}\right) \tag{2}$$

$$\lambda_t^{(o)} = \frac{x_t^{(o)} - x_t^{(l)}}{x_t^{(h)} - x_t^{(l)}},\ \lambda_t^{(c)} = \frac{x_t^{(c)} - x_t^{(l)}}{x_t^{(h)} - x_t^{(l)}} \tag{3}$$

$$x_t^{(o)} = \lambda_t^{(o)} x_t^{(h)} + \left(1 - \lambda_t^{(o)}\right) x_t^{(l)},\ x_t^{(c)} = \lambda_t^{(c)} x_t^{(h)} + \left(1 - \lambda_t^{(c)}\right) x_t^{(l)} \tag{4}$$

3. When the observed daily range is zero, the standard log-range and logit components are undefined. Following the transformation literature [50], a small, prespecified perturbation may be applied solely to make the transformation numerically defined. The perturbation rule, its magnitude, and the number of affected observations are necessary for

reproducibility; robustness depends on sensitivity to alternative perturbation magnitudes. A zero-range observation can coincide with a price-limit lock, but the transformation adjustment should not be interpreted as modeling whether orders could actually be executed on that day.

4. When $\lambda_t^{(o)}$ or $\lambda_t^{(c)}$ is equal to 0 or 1, it means that the open or close prices are equal to the highest or lowest prices. In order to satisfy the needs of empirical calculations, we used the tiny perturbation term to make $0 < \lambda_t^{(o)}, \lambda_t^{(c)} < 1$. When $\lambda_t^{(o)}$ or $\lambda_t^{(c)}$ is equal to 0, we increased $x_t^{(o)}$ or $x_t^{(c)}$ by p times to make $\lambda_t^{(o)}$ or $\lambda_t^{(c)}$ slightly larger than 0; when $\lambda_t^{(o)}$ or $\lambda_t^{(c)}$ is equal to 1, we reduced $x_t^{(o)}$ or $x_t^{(c)}$ by p times to make $\lambda_t^{(o)}$ or $\lambda_t^{(c)}$ slightly smaller than 1. Finally, we used logit change to make the range of its value become $(-\infty, +\infty)$ and obtain the unconstrained 3 and 4 terms:

$$y_t^{(3)} = \ln\left(\frac{\lambda_t^{(o)}}{1-\lambda_t^{(o)}}\right) \tag{5}$$

$$y_t^{(4)} = \ln\left(\frac{\lambda_t^{(c)}}{1-\lambda_t^{(c)}}\right) \tag{6}$$

Through the above transformation process, the original OHLC data X_t processing is transformed into the following unrestricted Y_t:

$$Y_t = \begin{pmatrix} y_t^{(1)} \\ y_t^{(2)} \\ y_t^{(3)} \\ y_t^{(4)} \end{pmatrix} = \begin{pmatrix} \ln x_t^{(l)} \\ \ln\left(x_t^{(h)} - x_t^{(l)}\right) \\ \ln\left(\frac{\lambda_t^{(o)}}{1-\lambda_t^{(o)}}\right) \\ \ln\left(\frac{\lambda_t^{(c)}}{1-\lambda_t^{(c)}}\right) \end{pmatrix}, \; y_t^{(i)} \in [-\infty, +\infty], \; i = 1,2,3,4 \tag{7}$$

$$X_t = \begin{pmatrix} x_t^{(o)} \\ x_t^{(h)} \\ x_t^{(l)} \\ x_t^{(c)} \end{pmatrix} = \begin{pmatrix} x_t^{(1)} \\ x_t^{(2)} \\ x_t^{(3)} \\ x_t^{(4)} \end{pmatrix} = \begin{pmatrix} \frac{e^{\left(y_t^{(2)} + y_t^{(3)}\right)}}{e^{y_t^{(3)}}+1} + e^{y_t^{(1)}} \\ e^{y_t^{(1)}} + e^{y_t^{(2)}} \\ e^{y_t^{(1)}} \\ \frac{e^{\left(y_t^{(2)} + y_t^{(4)}\right)}}{e^{y_t^{(4)}}+1} + e^{y_t^{(1)}} \end{pmatrix} \tag{8}$$

Each component of Y_t has a clear economic meaning and relevance: $y_t^{(1)}$ represents the lowest price level, $y_t^{(2)}$ measures a range-defined volatility, and $y_t^{(3)}$ and $y_t^{(4)}$ imply the extent to which the open and close prices are within the boundaries of the intraday price fluctuations. The above transformation process yields an unbounded size of Y_t that captures the intraday price movement and volatility well, and the original OHLC data X_t can be obtained after the inverse transformation.

3.2.2. Exchange-Imposed Price Limits and Forecast Feasibility

INE daily price limits constrain the maximum upward and downward movement relative to the preceding settlement price. By truncating the observed return distribution and suppressing some extreme movements, the mechanism can mechanically lower MAE, MSE/RMSE, and MAPE. Forecast errors obtained from INE prices therefore describe a regulated price process; a low error cannot by itself be interpreted as evidence that a model captures the market's unconstrained nonlinear volatility.

The unconstrained transformation preserves the internal OHLC ordering but does not impose the exchange-specific legal interval. An event-level robustness design should

reconstruct the upper and lower limits applicable on every trading day from the preceding settlement price and the contemporaneous contract rule; identify upper-limit, lower-limit, and locked-limit observations without using day-t information to forecast day t; and report model errors separately for normal and limit-affected observations. Execution analysis should additionally apply no-fill or carry-forward rules when counterparties are unavailable at a locked limit.

The available records do not include a verified historical schedule of changing INE price limits or a date-level limit-event series. Consequently, no event-level robustness result is reported in this paper, and GRU is described only as numerically best in the originally reported, institutionally constrained sample. The manuscript does not claim that the current ranking proves superior prediction of unconstrained crude-oil dynamics or limit-day execution feasibility.

3.2.3. Forecasting Models

Naive prediction method (Naive):

The naive forecasting method is one that directly uses the OHLC price of the previous day as a prediction of today's price without taking into account other influences, and of course derives from a similar method that uses the mean of the time prices of the past few days, which is suitable for forecasting relatively stationary time series:

$$\hat{Y}_t = Y_{t-1} \tag{9}$$

Multiple Linear Regression (MLR):

Multiple Linear Regression (MLR). The linear benchmark regresses the transformed four-dimensional OHLC target on prespecified lags of the transformed INE OHLC vector. No external financial variables enter the reported MLR or any of the six other forecasting specifications. All coefficients, scaling parameters, and lag-selection decisions should be estimated using the training block only.

$$\hat{Y}_t = \beta_0 + \beta_1 Y_{t-4:t-1} + \beta_2 X_{t-1} + \varepsilon_t \tag{10}$$

Vector Autoregressive Model and Vector Error Correction Model (VAR and VECM):

The VAR model proposed by Sims in 1980 is actually a set of multivariate linear regression equations [51], in which a specific variable p is selected to regress linearly on its own order lag terms, which can capture the dynamic linear relationship between variables very well. In the VAR model, $\Phi_0 \in \mathbb{R}^{4\times 1}$ is the intercept term, and $\Phi_i \in \mathbb{R}^{4\times 4}(1 \le i \le p)$ is the coefficient matrix of the corresponding lag order. However, the achievement of VAR model depends on the stationarity of the series, and for non-stationary time series, it is necessary to use Johansen test for the cointegration relationship [52]. So, Engle and Granger consider the correction of the cointegration systematic error for the non-stationary multiple time series for the first-order difference processing, and put forward the VECM model [53]. $\Gamma_{i-1}(1 \le i \le p)$ is the coefficient matrix obtained from Φ_i by obtaining the difference, α, $\beta \in \mathbb{R}^{4\times r}$, where β denotes the vector of cointegration, r is the cointegration of the order, and the time series $\beta^T Y_t$ is stationary. In the later empirical process, the VAR and VECM's window will be adjusted and a fixed number of days will be chosen as the period to roll forward for forecasting.

$$\hat{Y}_t = \Phi_0 + \Phi_1 Y_{t-1} + \Phi_2 Y_{t-2} + \cdots + \Phi_p Y_{t-p} + \varepsilon_t \tag{11}$$

$$\Delta\hat{Y}_t = \Gamma_0 + \sum_{j=1}^{p-1} \Gamma_j \Delta Y_{t-j} + \alpha\beta^T Y_{t-1} + \varepsilon_t \tag{12}$$

Support Vector Regression (SVR):

SVM was first proposed by Vapnik in 1988 [54]. This is a common supervised learning algorithm that aims to find a hyperplane to separate different samples and maximize the distance between the samples. The equation is as follows: $w^T x + b = 0$, where w denotes the normal vector. For the case of the definition of the domain on the (x_i, y_i), the hyperplane (w, b) is able to train the samples and classify them correctly; $w^T x + b > 0$ when $y_i = 1$; $w^T x + b < 0$ when $y_i = -1$; the interval $\gamma = 2/\|w\|$ is the sum of the distances from the dissimilar support vectors to the hyperplane; and in order to maximize the interval, the constraints of the optimization can be written as:

$$\min_{w,b} \frac{1}{2}\|w\|^2$$

$$\text{s.t. } y_i\left(w^T \boldsymbol{x}_i + b\right) \geq 1,\ i = 1, 2, \cdots, m \tag{13}$$

If the training samples are not linearly differentiable, we can use the mapping $\phi(\cdot)$ for the mapping of the original space to a higher-dimensional feature space. The feature space can be divided into hyperplane and can be expressed by the formula $f(x) = w^T \phi(x) + b$. Similarly to the linearly differentiable space, there is the following optimization problem; in order to calculate the solution of the following formula, for the convenience of the calculation, the construction of a kernel function is needed to represent the feature space of the inner product calculation:

$$\kappa(x_i, x_j) = < \phi(x_i), \phi(x_j) > = \phi(x_i)^T \phi(x_j) \tag{14}$$

$$\min_{w,b} \frac{1}{2}\|w\|^2$$

$$\text{s.t. } y_i\left(w^T \phi(x_i) + b\right) \geq 1,\ i = 1, 2, \cdots, m \tag{15}$$

Unlike the traditional regression model OLS, the support vector regression SVR assumes that losses are considered valid only when the absolute value of the difference between $f(x)$ and y exceeds a certain value, and by allowing some samples to fail to satisfy the constraint through soft margin, the SVR can be expressed as:

$$\min_{\boldsymbol{w},\boldsymbol{b}} \frac{1}{2}\|w\|^2 + C\sum_{i=1}^{m} L_\varepsilon(f(x_i) - y_i)$$

$$L_\varepsilon(f(x_i) - y_i) = \begin{cases} 0,\ |f(x_i) - y_i| \leq \varepsilon \\ |f(x_i) - y_i| - \varepsilon, |f(x_i) - y_i| > \varepsilon \end{cases} \tag{16}$$

Equation (16) defines the ε-insensitive loss used by SVR. Reproducibility depends on specifying the kernel, regularization parameter C, ε, scaling rule, and the time-ordered validation procedure used to choose them. Hyperparameters may not be selected according to performance on the final test period.

Convolutional Neural Networks (CNN):

Convolutional Neural Network (CNN) [55–59]. In this study, the CNN is used as a nonlinear sequence benchmark that extracts local patterns from the lagged transformed OHLC inputs. The relevant empirical choices are the input window, convolutional filters and kernel sizes, pooling operation, dense layers, PReLU activation, and four-dimensional output. These choices, rather than the generic history of CNNs, determine the reproducibility and fairness of the comparison.

$$f(x_i) = \begin{cases} x_i,\ x_i > 0 \\ a_i x_i,\ x_i \leq 0 \end{cases} \tag{17}$$

After convolution and pooling, the extracted features are flattened and mapped to the four transformed OHLC forecasts. Hyperparameters must be selected with the time-ordered validation block, and the final output must be inverse-transformed before computing price-scale errors. The specific framework is shown in Figure 6.

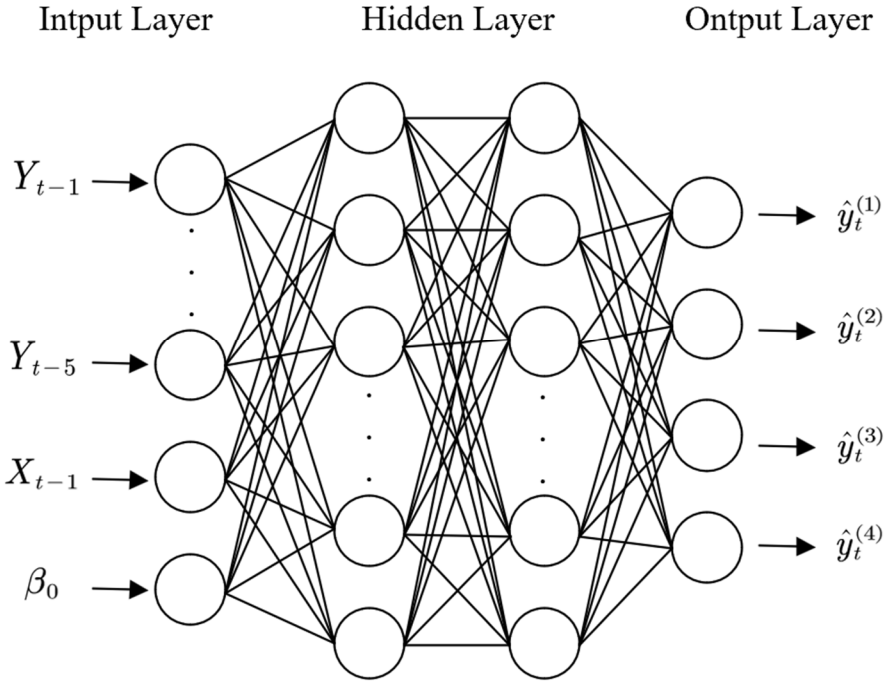

Figure 6. CNN structure diagram.

Long Short-Term Memory Network (LSTM):

Long Short-Term Memory Network (LSTM). LSTM [60] provides a recurrent benchmark for learning dependencies in the transformed OHLC sequence. Its input, forget, and output gates regulate the retained state, which may help model nonlinear temporal dependence. For this study, the essential implementation information is the input window, number of layers and hidden units, dropout, optimizer, batch size, stopping rule, random seed, and four-dimensional output; the available settings are outlined in Supplementary Table S1.

The LSTM state and gate updates used in the empirical implementation are summarized in Equations (18) and (19).

The values of the unit memory C_t, and the equations of the input gate I_t and the forget gate I_t are as follow:

$$\begin{aligned} \widetilde{C}_t &= \tanh(w_c[h_{t-1}, x_t] + B_c) \\ I_t &= \delta(w_i[h_{t-1}, x_t] + B_i) \\ f_t &= \delta\left(w_f[h_{t-1}, x_t] + B_f\right) \end{aligned} \tag{18}$$

In the above equation, w_c, w_i, and w_f denote the synthesized weight matrix; B_c, B_i, and B_f denote the synthesized deviations; h_{t-1} denotes the output value of the LSTM unit at the previous time step, and the input value y_t at moment t; tanh denotes the hyperbolic tangent activation function in the interval $(-1,1)$; and δ is the sigmoid activation function in the interval (0,1). The value of the unit memory C_t at moment t is calculated by the formula $C_t = f_t C_{t-1} + I_t \widetilde{C}_t$.

The value of the unit memory C_t at time t, depending on the last unit memory state C_{t-1}, is computed using the weight matrix w_0 of the output gate and the deviation B_0. The

value of the output gate is o_t and the corresponding output value of the LSTM unit h_t at time t is computed by the following equation:

$$o_t = \sigma(w_0[h_{t-1}, x_t] + B_0)$$

$$h_t = o_t tanh(C_t) \tag{19}$$

The LSTM forecasts are inverse-transformed to the OHLC price scale and evaluated using exactly the same time split, predictors, loss definition, and test observations as the competing models. The specific framework is shown in Figure 7.

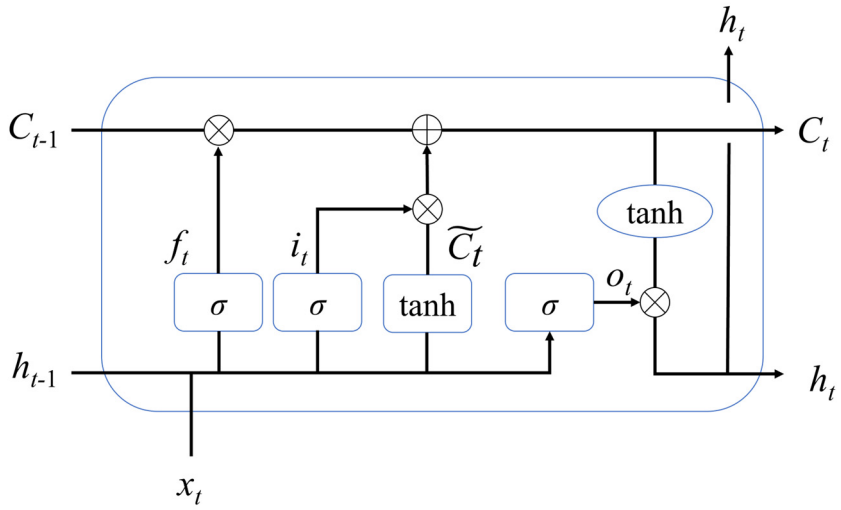

Figure 7. LSTM unit cell structure diagram.

Gated Recurrent Unit Network (GRU):

Unlike LSTM, GRU unifies the input and forget gates as update gates and performs both forgetting and selection memory using only one gating z_t [61,62], denoted by the following formula:

$$R_t = \sigma(W_r \times [h_{t-1}, x_t] + b_r)$$

$$Z_t = \sigma(W_u \times [h_{t-1}, x_t] + b_u)$$

$$C_t = \tanh(W_c \times [r_t \times h_{t-1}, x_t] + b_h)$$

$$H_t = (1 - z_t) \times h_{t-1} + z_t \times c_t$$

$$Y_t = \sigma(W_0 h_t) \tag{20}$$

In Equations (17)–(20), r_t and z_t denote the reset and update gates, respectively; c_t is the candidate hidden state; and h_t is the GRU hidden state. Because the transformed target $\hat{Y}_t$ has support on the real line, the output layer in Equation (20) is linear rather than sigmoid-bounded.

3.2.4. Forecast-Evaluation Design

Forecast accuracy should be reported separately for each component k in {Open, High, Low, Close}. For every model, MAE_k, RMSE_k, and MAPE_k are calculated from the component-specific observed and predicted price series on the same test observations. The equally weighted aggregate across the four components is retained only as a secondary symmetric summary of the complete OHLC vector; it is not an economic-value weighting and cannot substitute for the component-level results.

Interpretation should place particular emphasis on Close-price accuracy because Close is central to settlement, daily profit and loss, margin calculations, and subsequent-session decisions. High- and Low-price errors remain important for intraday range, stop-loss, take-profit, and risk assessment. A model should therefore not be selected for practical use solely from a 25–25–25–25% aggregate when its component-specific strengths and weaknesses are unknown.

The component-level prediction series required to calculate the Open-, High-, Low-, and Close-specific errors are not embedded in the manuscript or supplied as separate data files. The equal-weight aggregate is treated only as a secondary numerical summary and is not used to establish component-level or trading relevance.

$$MAE = \frac{1}{4n}\sum_{i=1}^{n}\sum_{j=1}^{4}\left|x_i^{(j)} - \hat{x}_i^{(j)}\right|$$

$$MSE = \frac{1}{4n}\sum_{i=1}^{n}\sum_{j=1}^{4}\left(x_i^{(j)} - \hat{x}_i^{(j)}\right)^2$$

$$RMSE = \sqrt{\frac{1}{4n}\sum_{i=1}^{n}\sum_{j=1}^{4}\left(x_i^{(j)} - \hat{x}_i^{(j)}\right)^2}$$

$$MAPE = \frac{1}{4n}\sum_{i=1}^{n}\sum_{j=1}^{4}\frac{\left|x_i^{(j)} - \hat{x}_i^{(j)}\right|}{x_i^{(j)}} \times 100\%$$

$$SR = \frac{1}{n}\sum\nolimits_{i=1}^{n}\frac{L\left(\hat{I}_t \cap I_t\right)}{L\left(\hat{I}_t \cup I_t\right)}, I_t = \left[x_t^{(3)}, x_t^2\right], \hat{I}_t = \left[\hat{x}_t^{(3)}, \hat{x}_t^2\right] \quad (21)$$

where I_t and $\hat{I}_t$ are the observed and forecast high-low intervals, and $|\cdot|$ denotes interval length. SR is therefore an interval-overlap measure, not a directional hit rate. It equals zero when the intervals do not overlap. The specific framework is shown in Figure 8.

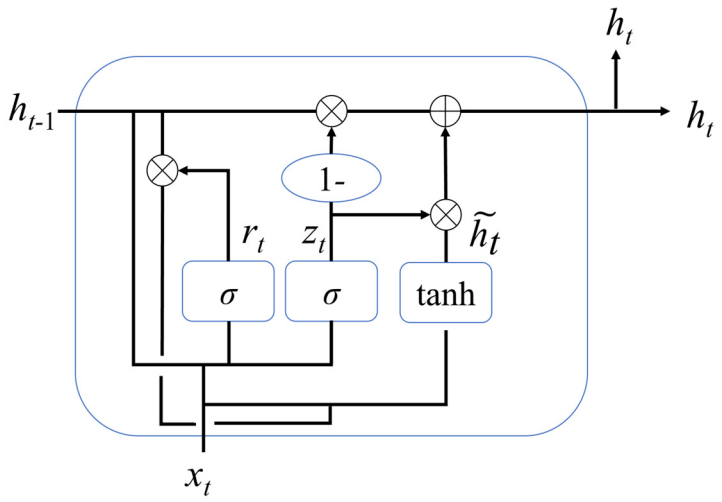

Figure 8. GRU unit cell structure diagram.

4. Forecasting Results

The archived materials report an 80:20 train-test ratio but do not identify the exact train and test dates, whether observations were shuffled, whether a separate validation block was used, or whether all scaling and preprocessing parameters were fitted exclusively on training observations. The current tables are therefore historical numerical comparisons

under an incompletely documented design rather than verified leakage-free out-of-sample results. A leakage-free evaluation must preserve chronology, use the earliest observations for estimation, reserve a subsequent block for hyperparameter selection and early stopping, leave the latest block untouched for one final evaluation, and fit every preprocessing operation on training data only. The OHLC-only empirical workflow is shown in Figure 9.

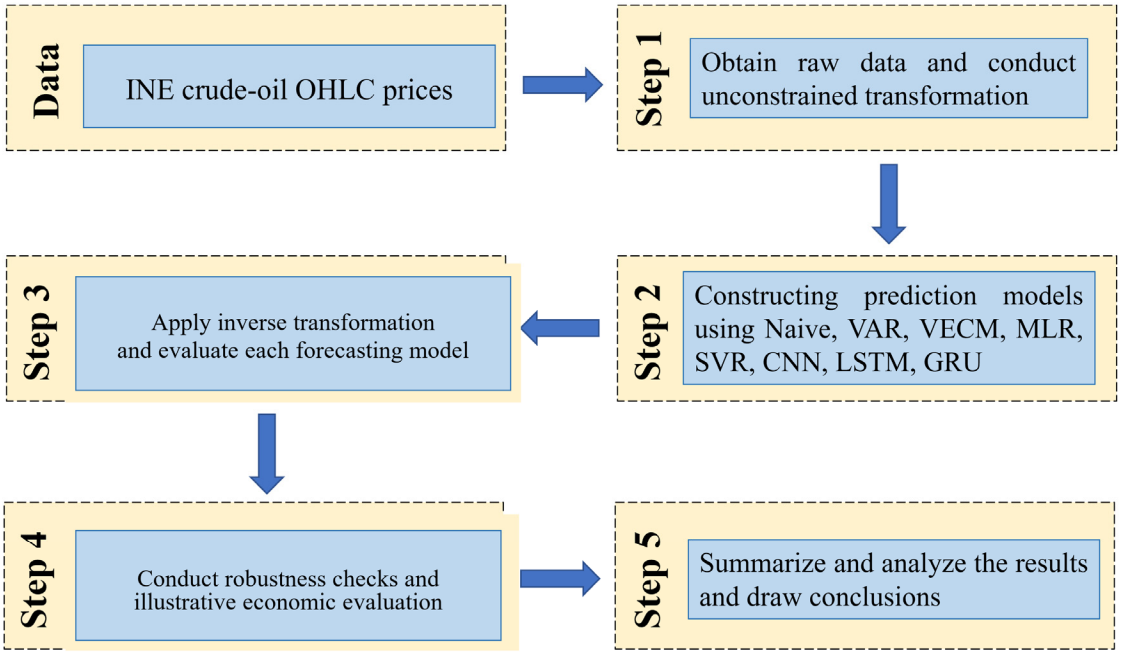

Figure 9. OHLC-only empirical workflow.

For VAR/VECM, stationarity and cointegration decisions should be made within each estimation window rather than from the full sample. Table 3 presents the currently reported comparison of rolling-window lengths. The window length must be chosen using training or validation data only; selecting it according to final test performance would contaminate the out-of-sample comparison. The ADF and Johansen specifications, deterministic terms, lag-order criterion, and re-estimation frequency support replication.

Table 3. Forecast accuracy of the VAR/VECM specification under alternative rolling-window lengths.

Rolling Window	MAPE	MAE	RMSE	SR
25	1.4096%	8.3745	12.0616	0.3698
30	1.3770%	8.1786	11.8576	0.3711
35	1.2985%	7.6857	10.8383	0.3812
40	1.2755%	7.5545	10.5704	0.3848
45	1.2693%	7.4999	10.4732	0.3913
50	1.2353%	7.2941	10.2357	0.3986
55	1.2080%	7.1358	10.1364	0.4057
60	1.2131%	7.1680	10.1504	0.4065

The nonlinear comparison includes SVR, CNN, LSTM, and GRU; MLR is a linear benchmark. The reported neural models use a look-back input denoted by step and a learning rate of 0.001, with mean squared error as the training loss. Training loss must be calculated on the training data, while validation loss may be used for early stopping. Test loss must not be used to update weights or select hyperparameters. The available implementation settings are outlined in Supplementary Table S1.

Table 4 retains the archived equal-weight aggregate results as a secondary benchmark. Because component-specific prediction series are not yet available, the table does not establish where each model performs well or poorly across Open, High, Low, and Close and is not used as standalone evidence of economic relevance.

Table 4. Secondary equal-weight aggregate errors on the originally reported test set.

Models	MAPE	MAE	RMSE	SR
Naive	1.2844%	7.5972	10.5490	0.3848
VAR and VECM	1.2080%	7.1358	10.1364	0.4057
MLR	1.1407%	6.7327	9.3154	0.4016
CNN	1.1144%	6.6290	9.5313	0.4609
SVR	0.9740%	5.7563	8.1862	0.4515
LSTM	0.8713%	5.1752	7.8007	0.5321
GRU	0.7825%	4.6774	7.2957	0.5629

Table 4 reports the archived equal-weight aggregate errors. The nonlinear models generally have lower numerical aggregates than the linear benchmarks, but the table does not reveal performance for Open, High, Low, or Close separately and does not establish economic usefulness.

GRU has the best numerical values in the current Table 4: MAPE of 0.7825%, MAE of 4.6774, RMSE of 7.2957, and SR of 0.5629. LSTM is second with MAPE of 0.8713%, MAE of 5.1752, RMSE of 7.8007, and SR of 0.5321. The relatively small GRU-LSTM difference should not be described as definitive superiority until paired loss differentials are tested and neural networks are re-estimated under multiple random seeds.

The main demonstrated advantage of the unconstrained transformation is structural: after inverse transformation, forecast OHLC values satisfy the internal ordering relationships by construction. This property prevents incoherent combinations such as a predicted low above the predicted high. It does not by itself guarantee compliance with exchange price limits, economic profitability, or robustness to structural breaks; those claims require the additional tests described above.

Figures 10 and 11 display the observed and currently reported predicted OHLC sequences for the original test period.

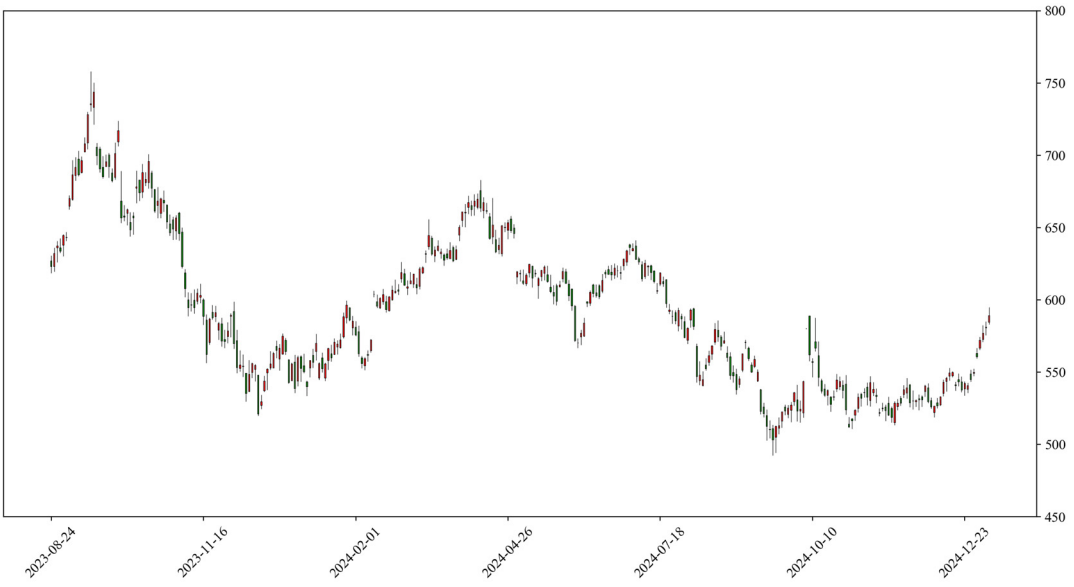

Figure 10. Observed INE crude-oil OHLC prices in the original test period. Note: Red indicates an increase, while green indicates a decrease.

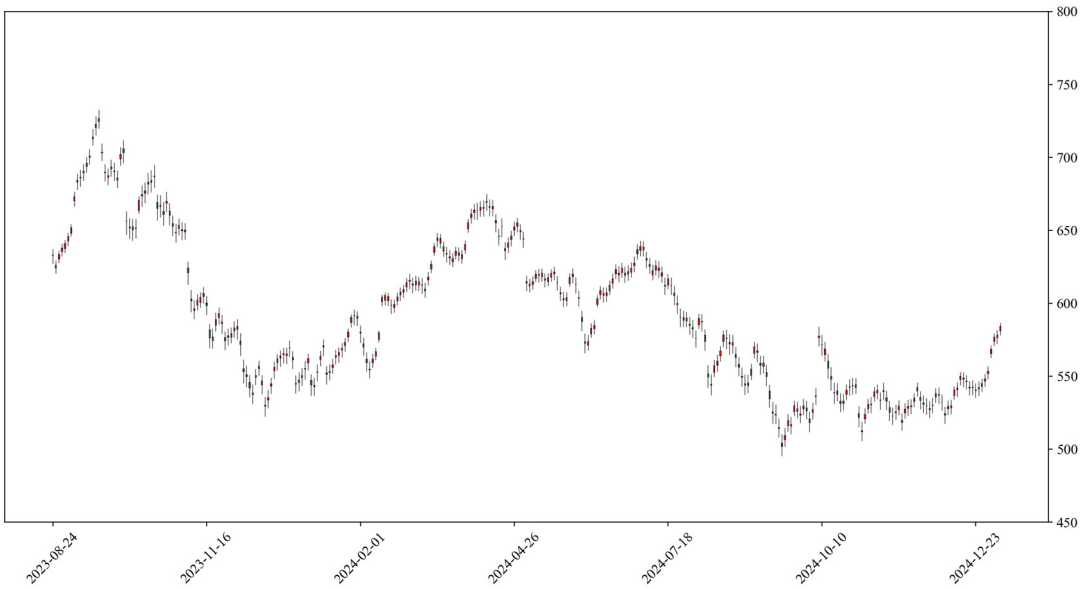

Figure 11. Currently reported predicted INE crude-oil OHLC prices in the original test period. Note: Red indicates an increase, while green indicates a decrease.

5. Robustness and Market-Regime Analysis

Table 5 reports the currently available 70:30 split as a sensitivity check. GRU remains numerically best, with MAPE of 0.8867%, MAE of 5.1645, RMSE of 7.5776, and SR of 0.5398. Changing a single split ratio does not, however, resolve regime dependence or demonstrate operational stability. The chronology and preprocessing protocol of the 70:30 specification have not been verified.

Table 5. Originally reported 70:30 sensitivity results.

Models	MAPE	MAE	RMSE	SR
Naive	1.3540%	7.7925	10.6200	0.3835
VAR and VECM	1.2994%	7.4604	10.3270	0.3936
MLR	1.3739%	7.9605	10.4170	0.2838
CNN	1.3524%	7.7989	10.5670	0.3981
SVR	1.1762%	6.8202	9.1732	0.3475
LSTM	0.8960%	5.1879	7.6726	0.5111
GRU	0.8867%	5.1645	7.5776	0.5398

Table 6 focuses on the 2020–2023 high-volatility period. Relative to the full-sample result in Table 4, GRU's reported MAPE rises from 0.7825% to 1.0215% (approximately 30.5%), MAE rises from 4.6774 to 6.0181 (approximately 28.7%), and RMSE rises from 7.2957 to 8.9433 (approximately 22.6%), while SR falls from 0.5629 to 0.5169. Thus, GRU remains numerically ahead of the listed competitors, but its accuracy deteriorates materially during market stress. This evidence supports a more cautious conclusion: low average error does not imply uniformly robust performance during the periods of greatest economic importance.

Table 7 varies the parameter labelled step, whose definition has not been verified. CNN performance is less stable than LSTM and GRU under the reported settings, while GRU remains numerically ahead. The economic interpretation depends on what step represents: an input look-back length and a multi-step forecast horizon are methodologically different experiments.

Table 6. Currently reported errors for the 2020–2023 high-volatility period.

Models	MAPE	MAE	RMSE	SR
Naive	1.5124%	8.8265	11.9610	0.3870
VAR and VECM	1.4951%	8.6846	11.8100	0.3593
MLR	1.3503%	8.0477	11.1670	0.4177
SVR	1.2246%	7.2568	10.3080	0.4467
CNN	1.4795%	8.6949	11.7965	0.3983
LSTM	1.0490%	6.2268	9.0395	0.5079
GRU	1.0215%	6.0181	8.9433	0.5169

Table 7. Sensitivity to the parameter labelled step.

Models	MAPE	MAE	RMSE	SR
CNN (step = 10)	1.0032%	5.9625	8.4553	0.4866
LSTM	0.8466%	5.0534	7.5401	0.5417
GRU	0.7846%	4.6924	7.3111	0.5455
CNN (step = 15)	1.4859%	8.7276	12.6046	0.3704
LSTM	0.8412%	5.0073	7.6273	0.5442
GRU	0.7991%	4.7710	7.2943	0.5533
CNN (step = 20)	0.9727%	5.7735	8.2684	0.4989
LSTM	0.8494%	5.0623	7.5476	0.5439
GRU	0.7941%	4.7319	7.2590	0.5603

6. Economic Evaluation of OHLC-Based Trading Rules

This section contains all definitions, calculations, and results for the economic exercise. It evaluates only two illustrative mappings: Close-to-Close and Open-to-Close. Neither is described as a validated or commercially implementable trading strategy because the archived analysis does not fully document the forecast cutoff, executable transaction price, bid-ask spread, slippage, rollover, financing, or position-management rules.

For Close-to-Close, the day-t closing-price forecast is compared with the observed closing price on day $t-1$; the forecast must be available before the execution decision. For Open-to-Close, the day-t forecast must be frozen before the market opens, the long or short signal must use only that forecast, and entry and exit prices must be defined ex ante. The reported calculations are illustrative mappings from forecasts to rules rather than evidence of attainable profitability.

Because daily OHLC observations do not reveal whether the low preceded the high, the former Low-to-High calculation is excluded from the reported economic results rather than treated as an executable strategy. The retained analysis therefore focuses on the Close-to-Close and Open-to-Close rules. The specific content is shown in Table 8.

Table 8. OHLC-based economic rules.

Economic Rule/Scenario	Triggers	Illustrative Operation
Close to close	$\hat{x}_t^{(c)} < \hat{x}_{t+1}^{(c)}$	Long position at the close price
Open to close	$\hat{x}_t^{(o)} < \hat{x}_t^{(c)}$	Long position at the open price and sell at the close price
	$\hat{x}_t^{(o)} > \hat{x}_t^{(c)}$	Short position at the open price and sell at the close price

Two OHLC-based rules are retained. (1) Under Close-to-Close, a long or short decision is formed from the day-t closing-price forecast relative to the observed day-$(t-1)$ close, subject to a prespecified execution time. (2) Under Open-to-Close, a long (short) position is

entered at an executable opening price when the forecast close is above (below) the forecast open and is closed according to a prespecified end-of-day rule. Both rules require strictly observable information and frozen parameters.

The exchange contract size and commissions are only part of trading cost. A realistic INE futures simulation must also account for bid-ask spreads, slippage, market impact, contract rollover, daily settlement, financing costs, changing margin requirements, margin calls, position limits, and forced liquidation. On price-limit days, an order at the theoretical limit price may remain unfilled because no counterparty is available. The current return calculation includes a simplified commission and constant-margin assumption only; its results should be interpreted as friction-light scenarios rather than attainable investor returns.

$$R_t = \frac{(P_2 - P_1) \times 1000 - F}{P_1 \times 1000 \times M} \times 100\% \quad (22)$$

For each rule, T denotes the number of trades, the number of positive trades provides a simple win count, and the mean and standard deviation summarize trade returns. The product $\prod(1 + R_t)$ is a terminal wealth multiple, not a net cumulative return or an annualized return. Net cumulative return equals $\prod(1 + R_t) - 1$; annualized return must be calculated separately from the elapsed test period. The Sharpe ratio [63] should be computed from a consistently sampled net return series after costs, using a risk-free rate aligned to the evaluation period rather than a single end-date yield. The reported calculations omit maximum drawdown, Calmar ratio, Sortino ratio, drawdown duration, turnover, and benchmark-relative performance [64].

$$\text{Mean daily net return} : \bar{r} = (1/N)\sum_{t=1}^{N} r_t$$

$$\text{Terminal wealth and cumulative return} : W = \prod_{t=1}^{N}(1 + r_t), CR = W - 1$$

$$\text{Daily volatility} : s = \sqrt{\left[(1/(N-1))\sum_{t=1}^{N}(r_t - \bar{r})^2\right]}$$

$$\text{Annualized Sharpe ratio} : [(\bar{r} - r_f, d)/s]\sqrt{242} \quad (23)$$

The Low-to-High sensitivity exercise is omitted because its trigger order cannot be verified from daily OHLC data and its adjustment factor was selected within the evaluation sample. It is not used to support the trading or investment conclusions.

Table 9 presents the archived unleveraged calculations for the two retained rules. The figures exclude several execution frictions and should be read only as simplified illustrative mappings, not as achieved arbitrage opportunities.

Table 9. Simplified unleveraged rule calculations before full execution costs.

Rule/Scenario	T	Positive Trades	Mean Return	Terminal Wealth Multiple	Std. Deviation	Sharpe Ratio
Close to Close	168	115	0.6425%	2.8595	0.0174	0.3594
Open to Close	309	205	0.4598%	4.0227	0.0129	0.3489

Table 10 applies the archived constant-20-margin assumption to the two retained rules. The resulting terminal wealth multiples reflect repeated compounding under simplified execution, reinvestment, and constant-margin assumptions while omitting slippage, market impact, financing, changing margin requirements, margin calls, and forced liquidation. They are idealized calculations and do not support an investment claim.

Table 10. Idealized constant-20–margin rule calculations before full execution constraints.

Rule/Scenario	T	Positive Trades	Mean Return	Terminal Wealth Multiple	Std. Deviation	Sharpe Ratio
Close to Close	168	115	3.2127%	105.8451	0.0872	0.3667
Open to Close	309	205	2.2989%	604.1932	0.0646	0.3543

Overall, the economic exercise shows how complete OHLC forecasts can be mapped to two candidate decision rules, but it does not demonstrate commercially implementable profitability. Close-to-Close and Open-to-Close remain illustrative until their forecast cutoff, execution prices, costs, and risk controls are fully specified. No result in this section supports an arbitrage claim or a long-term investment recommendation.

7. Conclusions and Limitations

This study asks whether an unconstrained, structure-preserving representation of daily OHLC prices can support coherent forecasting of INE crude-oil futures. Its central contribution is the preservation of the internal Open-High-Low-Close ordering while seven forecasting approaches are compared on a common numerical basis.

Under the originally reported 80:20 setting, GRU has the lowest equal-weight aggregate MAPE, MAE, and RMSE and the highest interval-overlap SR. That ranking is numerical rather than definitive: the exact temporal split and training-only preprocessing are not verified, component-specific errors are not yet available, and no price-limit-event robustness test is reported.

Section 6 provides only an illustrative bridge from full OHLC forecasts to Close-to-Close and Open-to-Close rules. Because execution timing and several trading frictions remain incompletely specified, these calculations do not establish investor-ready profitability. The forecasting comparison and the economic illustration therefore have distinct evidentiary roles and are not combined into a claim of validated trading performance.

Limitations. The archived analysis does not verify a leakage-free chronological split, training-only preprocessing, component-specific OHLC errors, or date-level price-limit robustness. The reported models are OHLC-only, the daily frequency does not reveal intraday execution order, and the economic calculations omit important execution frictions and downside-risk measures. These limitations restrict the conclusions to the structure-preserving representation and the numerical comparisons currently documented; broader claims about unconstrained market dynamics, practical profitability, liquidity, macroeconomic stability, enterprise resilience, or energy security are not supported.

Supplementary Materials: The following supporting information can be downloaded at: https://www.mdpi.com/article/10.3390/en19184428/s1, Table S1: Model architecture and training configuration (complete before resubmission).

Author Contributions: Conceptualization, W.Y.; Methodology, W.Y.; Software, W.Y.; Validation, W.Y.; Formal analysis, W.Y.; Investigation, W.Y.; Resources, Y.Z.; Data curation, Y.Z.; Writing—original draft, T.F.; Writing—review and editing, T.F.; Visualization, T.F.; Supervision, T.F. All authors have read and agreed to the published version of the manuscript.

Funding: This research was supported by National Science Found of China (Grant No. 71171083).

Institutional Review Board Statement: This article does not involve the ethical problem.

Data Availability Statement: Our data is sourced from SHANGHAI INTERNATIONAL ENERGY EXCHANGE, and the website address is https://www.ine.cn/index/othercontents/2026_Options/ (accessed on 5 September 2026).

Acknowledgments: We are thankful to the anonymous reviewers. We thank LetPub (www.letpub.com) for its linguistic assistance during the preparation of this manuscript.

Conflicts of Interest: Author Wenhao Yao is employed by the company Wanhua Chemical Group Co., Ltd. The remaining authors declare that the research was conducted in the absence of any commercial or financial relationships that could be construed as a potential conflict of interest.

References

1. Fan, Y.; Liang, Q.; Wei, Y.M. A generalized pattern matching approach for multi-step prediction of crude oil price. *Energy Econ.* **2008**, *30*, 3. [CrossRef]
2. Guo, L.L.; Huang, X.Y.; Li, Y.J.; Li, H.J. Forecasting crude oil futures price using machine learning methods: Evidence from China. *Energy Econ.* **2023**, *127*, 107089. [CrossRef]
3. Astveit, K.A. Oil price shocks in a data-rich environment. *Energy Econ.* **2014**, *45*, 268–279. [CrossRef]
4. Hamilton, J.D. Oil and the Macroeconomy since World War II. *J. Political Econ.* **1983**, *91*, 228–248. [CrossRef]
5. Ren, X.H.; He, Y.; Liu, C.W.; Tao, L.Z. Extreme risk spillovers between SC, WTI and Brent crude oil futures-Evidence from time-varying Granger causality test. *Energy* **2025**, *320*, 135495. [CrossRef]
6. Yi, A.D.; Yang, M.L.; Li, Y.S. Macroeconomic Uncertainty and Crude Oil Futures Volatility–Evidence from China Crude Oil Futures Market. *Front. Environ. Sci.* **2021**, *9*, 636903. [CrossRef]
7. Hu, J.F.; Xie, W.C.; Liu, M. How does digital village alleviate rural household energy poverty? *Energy* **2025**, *318*, 134713. [CrossRef]
8. Thi Huong Vuong, G.; Nguyen, M.H.; Hoang, K. Oil price uncertainty, oil pricing reform, and corporate profitability: The case of China. *PLoS ONE* **2024**, *19*, e0297554. [CrossRef] [PubMed]
9. Manickavasagam, J.; Visalakshmi, S.; Apergis, N. A novel hybrid approach to forecast crude oil futures using intraday data. *Technol. Forecast. Soc. Change* **2020**, *158*, 120126. [CrossRef] [PubMed]
10. Ji, Q.; Zhang, D.Y. China's crude oil futures: Introduction and some stylized facts. *Financ. Res. Lett.* **2019**, *28*, 376–380. [CrossRef]
11. Zhang, J.M.; Guo, S.L.; Dou, B.; Xie, B.Y. Evidence of the internationalization of China's crude oil futures: Asymmetric linkages to global financial risks. *Energy Econ.* **2023**, *127*, 107083. [CrossRef]
12. Yang, C.; Lv, F.; Fang, L.B.; Shang, X.X. The pricing efficiency of crude oil futures in the Shanghai International Exchange. *Financ. Res. Lett.* **2020**, *36*, 101329. [CrossRef]
13. Yu, Z.L.; Yang, J.; Webb, R.I. Price discovery in China's crude oil futures markets: An emerging Asian benchmark? *J. Futur. Mark.* **2022**, *43*, 297–324. [CrossRef]
14. Guo, Y.Q.; Zhang, S.C.; Liu, Y.Q. Research on Risk Features and Prediction of China's Crude Oil Futures Market Based on Machine Learning. *Front. Environ. Sci.* **2022**, *10*, 741018. [CrossRef]
15. Liu, M.; Lee, C.C. Capturing the dynamics of the China crude oil futures: Markov switching, co-movement, and volatility forecasting. *Energy Econ.* **2021**, *103*, 105622. [CrossRef]
16. Yang, K.; Wei, Y.; Li, S.W.; Liu, L.; Wang, L. Global financial uncertainties and China's crude oil futures market: Evidence from interday and intraday price dynamics. *Energy Econ.* **2021**, *96*, 105149. [CrossRef]
17. Yang, J.; Feng, Y.; Yang, H. The spillover and comovement of downside and upside tail risks among crude oil futures markets. *Int. Rev. Financ. Anal.* **2024**, *96*, 103578. [CrossRef]
18. Lan, Y.; Gao, H.X.; Zhou, P.; Zhang, H.; Li, H.L. The impact of climate risks on global energy production and consumption: New evidence from causality-in-quantile and wavelet analysis. *Energy* **2025**, *319*, 134850. [CrossRef]
19. Lyu, Y.J.; Wei, Y.; Hu, Y.Y.; Yang, M. Good volatility, bad volatility and economic uncertainty: Evidence from the crude oil futures market. *Energy* **2021**, *222*, 119924. [CrossRef]
20. Awartani, B.; Aktham, M.; Cherif, G. The connectedness between crude oil and financial markets: Evidence from implied volatility indices. *J. Commod. Mark.* **2016**, *4*, 56–69. [CrossRef]
21. Lin, B.Q.; Su, T. Do China's macro-financial factors determine the Shanghai crude oil futures market? *Int. Rev. Financ. Anal.* **2021**, *78*, 101953. [CrossRef]
22. Adedeji, A.N.; Ahmed, F.F.; Adam, S.U. Examining the dynamic effect of COVID-19 pandemic on dwindling oil prices using structural vector autoregressive model. *Energy* **2021**, *230*, 120813. [CrossRef] [PubMed]
23. Huang, W.Y.; Wang, H.W.; Qin, H.T.; Wei, Y.G.; Chevallier, J. Convolutional neural network forecasting of European Union allowances futures using a novel unconstrained transformation method. *Energy Econ.* **2022**, *110*, 106049. [CrossRef]
24. Shao, M.G.; Hua, Y.J. Price discovery efficiency of China's crude oil futures: Evidence from the Shanghai crude oil futures market. *Energy Econ.* **2022**, *112*, 106173. [CrossRef]
25. Wang, D.H.; Fang, T.H. Forecasting Crude Oil Prices with a WT-FNN Model. *Energies* **2022**, *15*, 1955. [CrossRef]
26. Yu, L.A.; Wang, Z.S.; Tang, L. A decomposition–ensemble model with data-characteristic-driven reconstruction for crude oil price forecasting. *Appl. Energy* **2015**, *156*, 251–267. [CrossRef]

27. Fang, T.H.; Zheng, C.L.; Wang, D.H. Forecasting the crude oil prices with an EMD-ISBM-FNN model. *Energy* **2023**, *263*, 125407. [CrossRef]
28. Sun, S.L.; Sun, Y.Y.; Wang, S.Y.; Wei, Y.J. Interval decomposition ensemble approach for crude oil price forecasting. *Energy Econ.* **2018**, *76*, 274–287. [CrossRef]
29. Sun, Y.Y.; Han, A.; Hong, Y.M.; Wang, S.Y. Threshold autoregressive models for interval-valued time series data. *J. Econom.* **2018**, *206*, 414–446. [CrossRef]
30. Sun, W.X.; Chen, H.L.; Liu, F.; Wang, Y. Point and interval prediction of crude oil futures prices based on chaos theory and multiobjective slime mold algorithm. *Ann. Oper. Res.* **2025**, *345*, 1003–1033. [CrossRef] [PubMed]
31. Yang, K.; Xu, X.Q.; Wei, Y.J.; Wang, S.Y. Forecasting interval-valued returns of crude oil: A novel kernel-based approach. *J. Forecast.* **2024**, *43*, 2937–2953. [CrossRef]
32. Wang, P.; Gurmani, S.H.; Tao, Z.F.; Liu, J.P.; Chen, H.Y. Interval time series forecasting: A systematic literature review. *J. Forecast.* **2024**, *43*, 249–285. [CrossRef]
33. Leitch, G.; Tanner, J. Economic forecast evaluation: Profits versus the conventional error measures. *Am. Econ. Rev.* **1991**, *81*, 580–590.
34. Chai, J.; Xing, L.M.; Zhou, X.Y.; Zhang, Z.G.; Li, J.X. Forecasting the WTI crude oil price by a hybrid-refined method. *Energy Econ.* **2018**, *71*, 114–127. [CrossRef]
35. Moshiri, S.; Foroutan, F. Forecasting nonlinear crude oil futures prices. *Energy J.* **2006**, *27*, 81–95. [CrossRef]
36. Wu, W.; Xu, M.Q.; Su, R.Q.; Ullah, K. Modeling crude oil volatility using economic sentiment analysis and opinion mining of investors via deep learning and machine learning models. *Energy* **2024**, *289*, 130017. [CrossRef]
37. Wu, H.L.; Li, P.; Cao, J.W.; Xu, Z.J. Forecasting the Chinese crude oil futures volatility using jump intensity and Markov-regime switching model. *Energy Econ.* **2024**, *134*, 107588. [CrossRef]
38. Niu, Z.B.; Liu, Y.Y.; Gao, W.; Zhang, H.W. The role of coronavirus news in the volatility forecasting of crude oil futures markets: Evidence from China. *Resour. Policy* **2021**, *73*, 102173. [CrossRef] [PubMed]
39. Zhang, Y.J.; Ma, F.; Shi, B.S.; Huang, D.S. Forecasting the prices of crude oil: An iterated combination approach. *Energy Econ.* **2018**, *70*, 472–483. [CrossRef]
40. Yi, Y.S.; Ma, F.; Zhang, Y.J.; Huang, D.S. Forecasting the prices of crude oil using the predictor, economic and combined constraints. *Econ. Model.* **2018**, *75*, 237–245. [CrossRef]
41. Yang, Q.; He, K.J.; Wu, D.C.W.; Zou, Y.C. China's Crude oil futures forecasting with search engine data. *Procedia Comput. Sci.* **2022**, *214*, 965–972. [CrossRef]
42. Wen, D.Y.; Wang, Y.D.; Zhang, Y.J. Intraday return predictability in China's crude oil futures market: New evidence from a unique trading mechanism. *Econ. Model.* **2021**, *96*, 209–219. [CrossRef]
43. Zhang, Q.; Di, P.; Farnoosh, A. Study on the impacts of Shanghai crude oil futures on global oil market and oil industry based on VECM and DAG models. *Energy* **2021**, *223*, 120050. [CrossRef]
44. Li, X.R.; Shang, W.; Wang, S.Y. Text-based crude oil price forecasting: A deep learning approach. *Int. J. Forecast.* **2019**, *35*, 1548–1560, Erratum in *Int. J. Forecast.* **2021**, *37*, 1312–1313. [CrossRef]
45. Zhai, D.S.; Zhang, T.R.; Liang, G.Q.; Liu, B.L. Research on crude oil futures price prediction methods: A perspective based on quantum deep learning. *Energy* **2025**, *320*, 135080. [CrossRef]
46. Jiang, Z.; Zhang, L.; Zhang, L.L.; Wen, B. Investor sentiment and machine learning: Predicting the price of China's crude oil futures market. *Energy* **2022**, *247*, 123471. [CrossRef]
47. He, K.J.; Yu, L.A.; Zou, Y.C. Crude oil future price forecasting using pretrained transformer model. *Procedia Comput. Sci.* **2024**, *242*, 288–293. [CrossRef]
48. Luo, H.; Yu, Y. A novel hybrid forecasting system for crude oil futures prices: A dual perspective of deterministic forecasting and uncertainty analysis. *Heliyon* **2024**, *10*, e39818. [CrossRef] [PubMed]
49. Sun, Y.; Yuan, X. Nonlinear relationship between money market rate and stock market liquidity in China: A multifractal analysis. *PLoS ONE* **2021**, *16*, e0249852. [CrossRef] [PubMed]
50. Huang, W.Y.; Wang, H.W.; Wang, S.S. A structural VAR and VECM modeling method for open-high-low-close data contained in candlestick chart. *Financ. Innov.* **2024**, *10*, 97. [CrossRef]
51. Sims, C. Macroeconomics and reality. *Econometrica* **1980**, *48*, 1–48. [CrossRef] [PubMed]
52. Johansen, S. Statistical analysis of cointegration vectors. *J. Econ. Dyn. Control* **1988**, *12*, 231–254. [CrossRef]
53. Engle, R.; Granger, C. Cointegration and Error Correction Representation, Estimation and Testing. *Econometrica* **1987**, *55*, 251–276. [CrossRef]
54. Vapnik, V.N. *Statistical Learning Theory (Adaptive and Learning Systems for Signal Processing, Communications and Control)*; Wiley: New York, NY, USA, 1998.
55. Fukushima, K.N. A self-organizing neural network model for a mechanism of pattern recognition unaffected by shift in position. *Biol. Cybern.* **1980**, *36*, 193–202. [CrossRef] [PubMed]

56. Wang, Z.J.; Turko, R.; Shaikh, O.; Park, H.; Das, N.; Hohman, F.; Kahng, M.; Polo Chau, D.H. CNN Explainer: Learning Convolutional Neural Networks with Interactive Visualization. *IEEE Trans. Vis. Comput. Graph.* **2021**, *27*, 1396–1406. [CrossRef] [PubMed]
57. Gudelek, M.U.; Boluk, S.A.; Ozbayoglu, A.M. A deep learning based stock trading model with 2-D CNN trend detection. In Proceedings of the 2017 IEEE Symposium Series on Computational Intelligence, Honolulu, HI, USA, 27 November–1 December 2017; pp. 1–8. [CrossRef]
58. Hoseinzade, E.; Haratizadeh, S. CNNpred: CNN-based stock market prediction using a diverse set of variables. *Expert Syst. Appl.* **2019**, *129*, 273–285. [CrossRef]
59. Xu, Z.M.; Wang, Y.J.; Feng, X.T.; Wang, Y.L.; Li, Y.L.; Lin, H. Quantum-enhanced forecasting: Leveraging quantum gramian angular field and CNNs for stock return predictions. *Financ. Res. Lett.* **2024**, *67*, 105840. [CrossRef]
60. Hochreiter, S.; Schmidhuber, J. Long Short-Term Memory. *Neural Comput.* **1997**, *9*, 1735–1780. [CrossRef] [PubMed]
61. Kamo, T.; Dagli, C. Hybrid approach to the Japanese candlestick method for f inancial forecasting. *Expert Syst. Appl.* **2009**, *36*, 5023–5030. [CrossRef]
62. Chung, J.; Gulcehre, C.; Cho, K.; Bengio, Y. Empirical evaluation of gated recurrent neural networks on sequence modeling. NIPS 2014 Workshop on Deep Learning. *arXiv* **2014**, arXiv:1412.3555.
63. Kan, R.; Wang, X.L.; Zheng, X.H. In-sample and out-of-sample Sharpe ratios of multi-factor asset pricing models. *J. Financ. Econ.* **2024**, *155*, 103837. [CrossRef]
64. Fama, E.F.; French, K.R. A five-factor asset pricing model. *J. Financ. Econ.* **2015**, *116*, 1–22. [CrossRef]

Disclaimer/Publisher's Note: The statements, opinions and data contained in all publications are solely those of the individual author(s) and contributor(s) and not of MDPI and/or the editor(s). MDPI and/or the editor(s) disclaim responsibility for any injury to people or property resulting from any ideas, methods, instructions or products referred to in the content.